Aust. J. Phys., 1984, **37**, 179–95

The Influence of Vertical Vorticity on Thermal Convection

J. O. Murphy and J. M. Lopez

Department of Mathematics, Monash University,
Clayton, Vic. 3168.

Abstract

The single-mode equations of Boussinesq thermal convection have been modified to include the vertical component of vorticity, which has led, in certain parameter ranges, to a new family of solutions for stationary convection in the absence of external constraints. The features of these solutions are discussed and a comparison with the family of solutions possessing zero vertical vorticity, which are also solutions of the equations, is presented. Specifically, these new solutions are characterized by a lower vertical velocity and heat flux, nonzero vertical vorticity thereby giving them a helical structure and considerably reduced thermal boundary layers in comparison with the family of solutions with zero vertical vorticity. It is to be stressed that this new family of solutions is not due to externally applied influences such as rotation or a magnetic field, the only driving force present being that due to buoyancy.

1. Introduction

Within the framework of the single horizontal mode approach to Rayleigh–Benard convection it is established that the vertical component of vorticity, which is usually neglected in studies of this type, has a profound effect on the nature of steady-state thermal convection, especially in fluids with small Prandtl numbers. It has been shown (Chandrasekhar 1961) that the second order differential equation describing the vertical vorticity decouples from the rest of the differential system when calculating the critical Rayleigh numbers at the marginal state for the onset of stationary convection in the linear case and, when solved together with the boundary conditions (be they rigid or stress-free), the vertical component of vorticity is identically zero. Consequently, the vertical vorticity has no effect on the velocity or temperature fluctuation at the marginal state. Stuart (1964) has emphasized that, when $(R-R_c)/R_c \ll 1$, the spatial patterns realized from the nonlinear theory are identical with those of the linearized theory and, accordingly, when the system is near the marginal state it will have no vertical vorticity. In the results presented here, obtained from the nonlinear system of equations which include the vertical vorticity terms, it is also found that the vertical vorticity vanishes for parameter values near the marginal state. However, Busse (1972) indicated that the usual analysis, based upon an expansion in powers of the amplitude ε of convection as a small parameter, has little relevance in the limit of low Prandtl number because it neglects some important nonlinear terms, in particular those of the vertical vorticity in the equation of motion.

0004-9506/84/020179$02.00

The importance of these terms relative to other nonlinear terms in the heat equation, as the Prandtl number decreases, has also been established in this investigation.

The modal approach employed here expands the velocity, vorticity and fluctuating temperature in terms of the horizontal eigenfunctions from the linear theory which are truncated to retain the first mode. This approach has often been used, for example by Van der Borght and Murphy (1973), Gough *et al.* (1975) and Latour *et al.* (1981); however, in the second and third studies the vertical vorticity has been ignored altogether. In the first study the choice of planform led to a system which is independent of the Prandtl number and the vertical vorticity is generated solely through the external effects of rotation and a magnetic field, the so-called mean-field equations. Time-dependent studies of the single-mode equations, with a hexagonal planform and with no externally imposed forces such as rotation or magnetic fields, have always led to a steady state when R exceeds some critical value R_c, and no bifurcations from this state have been detected.

Baker and Spiegel (1975) made a single-mode study in hexagonal planform of the hydrodynamic-convection equations with rotation and found two distinct types of solutions, one with comparatively large vertical velocities, of the type found by Gough *et al.* (1975) in ordinary Rayleigh–Benard convection, and another which has a greatly reduced vertical velocity together with a marked increase in the vertical vorticity. Also, a change in the sense of twisting of the fluid was noted; in the first type of solution the vertical vorticity is negative throughout the layer, while in the second type it is positive except in a small part near the top of the layer. Van der Borght (1976) also found these two types of solutions when solving single-mode equations in the presence of rotation combined with a vertical magnetic field. Lopez and Murphy (1982) studied the time-dependent magneto-convection equations without rotation and, for certain parameter values, found that the equivalent of the first type of solutions given by Van der Borght (1976), referred to as type I, were a transient solution which evolved on further time integration into the second type II solutions. With the inclusion of so many interactive effects, it is difficult to isolate the particular causes inducing this second type of solution which, incidently, has not been detected in other studies of single-mode equations (Toomre *et al.* 1976; Latour *et al.* 1976). The question is raised as to whether or not the existence of the type II solutions is solely due to the external effects of rotation or a magnetic field. Here the system has been depleted of these external effects in order to identify the origin of the type II solutions, while retaining the vertical component of the vorticity. In fact, the only difference between the equations examined here and those in Gough *et al.* (1975) is the inclusion of the vertical vorticity; it is demonstrated that the inclusion of a nonlinear vertical vorticity term in the momentum equation and the addition of a differential equation for the vertical vorticity, which increases the overall order of the system by two, is all that is needed to supplement the Gough *et al.* (1975) system for type II solutions to be possible within certain parameter ranges.

The attractiveness of the type II solutions, which are characterized by a velocity structure with nonzero helicity defined by $H_0 = \langle \boldsymbol{u} . \boldsymbol{\omega} \rangle$, where angle brackets indicate integration over a cell volume, is that for the same set of parameters they do not possess the sharp thermal boundary layers which are associated with type I solutions. These boundary layers have often been thought of as unstable and an artificial consequence of the single-mode equations (Toomre *et al.* 1977; Zahn *et al.* 1982).

Also, Toomre *et al.* (1977) reported that type I solutions possess a 'bump' in the mean temperature profile near the lower boundary which they regarded as being unstable. With type II, this bump is no longer present on the mean temperature profile.

The existence of type II solutions is of particular relevance to stellar convection, where the Rayleigh number is large ($\sim 10^{12}$) and the Prandtl number, due to radiative cooling, is low ($\sim 10^{-6} - \sim 10^{-9}$), since it is precisely at these extremes of these parameters that the type II solutions manifest themselves most strongly.

In the next section, the relevant equations are set out, and a discussion of the geometric significance of the velocity structure employed is given, as well as a description of the method of solution. In Section 3 the numerical results are presented, as well as a comparison between the type I and type II solutions. Finally, in Section 4, implications are discussed and conclusions drawn.

2. Equations

The physical set up of the problem is that of an infinite layer of fluid of depth d, with a coefficient of thermal diffusivity κ, coefficient of volume expansion α and viscous diffusivity ν, and which is heated from below. The upper and lower boundaries are maintained at constant temperatures, the difference between them being ΔT. The fluid is taken to be the Boussinesq type, so that density fluctuations are solely due to buoyancy effects. The general equations governing this system are (Chandrasekhar 1961)

$$\text{Continuity:} \qquad \partial\rho/\partial t + \nabla.(\rho \boldsymbol{u}) = 0, \tag{1}$$

$$\text{Momentum:} \qquad \rho\partial \boldsymbol{u}/\partial t + \rho \boldsymbol{u}.\nabla \boldsymbol{u} + \nabla P - \rho \boldsymbol{G} - \mu\nabla^2 \boldsymbol{u} = 0, \tag{2}$$

$$\text{Heat:} \qquad \rho C_V \partial T/\partial t + \rho C_V \boldsymbol{u}.\nabla T - K\nabla^2 T = 0, \tag{3}$$

where ρ is the density, μ the viscosity, K the conductivity, C_V the specific heat at constant volume, $\boldsymbol{u}$ the velocity, T the temperature, P the pressure and $\boldsymbol{G} = (0, 0, g)$, with g the acceleration due to gravity. Since the flow is the Boussinesq type, the continuity equation becomes $\nabla.\boldsymbol{u} = 0$.

The equations are then used to derive the single-mode equations from a variational method following the procedure of Van der Borght and Murphy (1973). The following expressions are adopted:

$$\boldsymbol{u} = \big((1/k^2)\{\mathrm{D}W(z)\partial f/\partial x + Z(z)\partial f/\partial y\}, \\ (1/k^2)\{\mathrm{D}W(z)\partial f/\partial y - Z(z)\partial f/\partial x\}, W(z)f\big), \tag{4}$$

$$T = T_0(z) + F(z)f, \tag{5}$$

$$\rho = \rho_0(z) + \rho^*(z)f, \tag{6}$$

$$P = P_0(z) + \pi(z)f, \tag{7}$$

for the dependent variables, where $\mathrm{D} \equiv \mathrm{d}/\mathrm{d}z$, W is the vertical component of velocity, Z the vertical component of vorticity, T_0 the mean temperature across the layer,

F the temperature fluctuation, ρ_0 the mean density, ρ^* the density fluctuation, P_0 the mean pressure and π the pressure fluctuation, all being functions of the vertical coordinate z. The planform function f is the horizontal linear eigenfunction which satisfies the equation

$$\partial^2 f(x,y)/\partial x^2 + \partial^2 f(x,y)/\partial y^2 = -k^2 f(x,y), \tag{8}$$

and k is the horizontal wavenumber. The particular f which is employed here is that due to Christopherson (1940) which describes a hexagonal planform.

Since the role of the vertical vorticity has been identified as the crucial factor in establishing the type II solutions, it is necessary to clearly emphasize the effects of including Z in the horizontal components of $\boldsymbol{u}$, given in (4). Firstly, the continuity equation $\nabla . \boldsymbol{u} = 0$ is automatically satisfied when the fluid velocity is given by the more general expression (4) for the velocity. Secondly, the inclusion of the $Z(z)$ terms in (4) now gives the fluid an extra degree of freedom in as much as they allow a vertical component of vorticity to be taken into account. There is no physical reason *a priori* why it should be assumed that the vertical vorticity vanishes and, in fact, as is found in this study, it is nonzero over certain parameter ranges. Thirdly, as a derived quantity, vorticity is always present, i.e. $\boldsymbol{\omega} = \nabla \times \boldsymbol{u}$, and in this case it takes the component form

$$\begin{aligned}\boldsymbol{\omega} = \big((1/k^2)\{\mathrm{D}Z(z)\partial f/\partial x - (\mathrm{D}^2 - k^2)W(z)\partial f/\partial y\}, \\ (1/k^2)\{\mathrm{D}Z(z)\partial f/\partial y + (\mathrm{D}^2 - k^2)W(z)\partial f/\partial x\}, Z(z)f\big),\end{aligned} \tag{9}$$

from which it is readily seen that if the term $Z \equiv 0$ in the expression for the velocity given by (4), then the vertical component of vorticity vanishes from (9). The helicity, which is a closely related quantity, takes the form

$$\begin{aligned} H_0 &= \langle \boldsymbol{u} . \boldsymbol{\omega} \rangle \\ &= \int_0^d \{(1/k^2)\mathrm{D}W(z)\mathrm{D}Z(z) - (1/k^2)Z(z)(\mathrm{D}^2 - k^2)W(z) + W(z)Z(z)\}\,\mathrm{d}z, \end{aligned} \tag{10}$$

which also vanishes when $Z \equiv 0$.

The relevant equations (non-dimensionalized) are

$$(\mathrm{D}^2 - a^2)Z = (C/\sigma)(W\mathrm{D}Z - Z\mathrm{D}W), \tag{11}$$

$$(\mathrm{D}^2 - a^2)^2 W = Ra^2 F + (C/\sigma)\{W(\mathrm{D}^2 - a^2)\mathrm{D}W + 2\mathrm{D}W(\mathrm{D}^2 - a^2)W + 3Z\mathrm{D}Z\}, \tag{12}$$

$$(\mathrm{D}^2 - a^2)F = W\mathrm{D}T_0 + C(2W\mathrm{D}F + F\mathrm{D}W), \tag{13}$$

$$\mathrm{D}^2 T_0 = \mathrm{D}(FW), \tag{14}$$

where $R = g\alpha d^3 \Delta T/\kappa\nu$ is the Rayleigh number, $\sigma = \nu/\kappa$ is the Prandtl number, $a = kd$ is the horizontal wavenumber and C, in the case of a hexagonal planform, takes the value $\sqrt{\frac{1}{6}}$.

In this paper equations (4), (11) and (12) differ from those published by Gough *et al.* (1975) and Toomre *et al.* (1977) in as much as they have taken the vertical

vorticity $Z \equiv 0$, and yet, the inclusion of the $3ZDZ$ term, which is a nonlinear modification of the momentum equation (12), clearly increases in importance as σ is decreased. The steady-state equations, as given by (11)–(14), have been specifically employed at this stage in order to isolate the effects of including the vertical vorticity in the single-mode system and to demonstrate the existence of two distinct types of steady-state solutions associated with this system of equations.

The geometrical consequence of including Z, on the flow structure, is significant. The stream lines of a hexagonal cell where $Z \equiv 0$ (Stuart 1964) clearly show that the fluid is confined within triangular prisms, across whose boundaries there is no flow, twelve of these prisms making up a hexagonal cell. A discussion of related geometric aspects associated with hexagonal cellular patterns has been given by Chandrasekhar (1961). Yet, when provision is made for the vertical vorticity to modify the velocity components, as in equation (4), horizontal twisting is then permitted and the flow is no longer confined within these triangular prisms, giving it the true characteristics of hexagonal cellular structure.

The free-surface boundary conditions have been employed in conjunction with equations (11)–(14). These specifications on the dependent variables on the upper and lower boundaries are

$$W(z=0) = W(z=1) = 0, \tag{15a}$$

$$\mathrm{D}^2 W(z=0) = \mathrm{D}^2 W(z=1) = 0, \quad \mathrm{D}Z(z=0) = \mathrm{D}Z(z=1) = 0, \tag{15b,c}$$

$$F(z=0) = F(z=1) = 0, \quad T_0(z=0) = 0, \quad T_0(z=1) = -1. \tag{15d,e,f}$$

This complete nonlinear differential system of order 10 has been solved using a collocation method in which the variables are expanded in either a Fourier sine or cosine series, depending on the corresponding boundary conditions, using

$$W(z) = \sum_{n=1}^{M} W_n \sin(n\pi z), \qquad Z(z) = L_0 + \sum_{n=1}^{M} L_n \cos(n\pi z), \tag{16a,b}$$

$$F(z) = \sum_{n=1}^{M} f_n \sin(n\pi z), \qquad T_0(z) = -z + \sum_{n=1}^{M} t_n \sin(n\pi z). \tag{16c,d}$$

The inclusion of the L_0 term in the cosine expansion for the vertical vorticity is an essential feature of the analysis.

When these expansions (16), together with the scalings $R_1 = R/\pi^4$, $\omega_n = W_n/\pi^2$ and $\alpha = a/\pi$, are substituted into equations (11)–(14), the following system of nonlinear algebraic equations for the coefficients results:

$$(n^2+\alpha^2)^2\omega_n - R_1\alpha^2 f_n + \frac{3C}{\sigma\pi^5} n L_0 L_n$$

$$+\frac{C\pi}{2\sigma}\sum_{p=1}^{M}\omega_p\{|n-p|(3\alpha^2+3p^2+n^2-2np)\omega_{|n-p|}-(n+p)(3\alpha^2+3p^2+n^2+2np)\omega_{n+p}\}$$

$$+\frac{3C}{2\sigma\pi^5}\sum_{p=1}^{M} L_p\{|n-p|L_{|n-p|}+(n+p)L_{n+p}\} = 0, \tag{17}$$

$$(n^2+\alpha^2)f_n - \omega_n - \tfrac{1}{2}\pi \sum_{p=1}^{M} \omega_p\{(n+p)t_{n+p} - |n-p|\, t_{|n-p|}\}$$

$$-\tfrac{1}{2}C\pi \sum_{p=1}^{M} \omega_p\{(2n+p)f_{n+p} + Y(p-n)(2n-p)f_{|n-p|}\} = 0, \quad (18)$$

$$nt_n - \tfrac{1}{2}\pi \sum_{p=1}^{M} \omega_p\{f_{n+p} + Y(p-n)f_{|n-p|}\} = 0, \quad (19)$$

$$(n^2+\alpha^2)L_n - \frac{C\pi}{\sigma} nL_0\,\omega_n - \frac{C\pi}{2\sigma} \sum_{p=1}^{M} \omega_p\{(2p+n)L_{n+p} + (2p-n)L_{|n-p|}\} = 0, \quad (20)$$

$$\alpha^2 L_0 - \frac{C\pi}{\sigma} \sum_{p=1}^{M} pL_p\,\omega_p = 0, \quad (21)$$

where

$$\begin{aligned} Y(n) &= 1, \quad n > 0 \\ &= 0, \quad n = 0 \\ &= -1, \quad n < 0. \end{aligned} \quad (22)$$

The generalized Newton–Raphson method has been utilized to solve the system (17)–(21). The number of collocation points M required across the layer $0 \leqslant z \leqslant 1$ depends essentially on the value of R and was typically between 60 and 90. Overall, the choice of M for any particular set of parameters must ensure constancy across the layer of the Nusselt number N, which is the first integral of equation (14), given by

$$N = FW - \mathrm{D}T_0. \quad (23)$$

This non-dimensional measure of the heat flux has the value $N = 1$ in the absence of energy transport by convective processes, and when the boundary conditions are taken into account, the following expression results:

$$N = 1 + \int_0^1 FW\,\mathrm{d}z. \quad (24)$$

3. Numerical Results

The system of equations described in the previous section clearly depends on a number of parameters. The Rayleigh and Prandtl numbers describe the physical properties of the fluid, whereas a and C describe the geometric features of the flow. A complete survey of the multiple parameter space is beyond the scope of this study. Consequently we have taken $a = \pi$ and the planform parameter C has been chosen to represent hexagonal cells with the value $\sqrt{\frac{1}{6}}$, although some $C = 0$ solutions, which follow from the mean-field equations, are included for comparison. The physical parameters R and σ, however, have been surveyed extensively, and trends evident at extreme values of these quantities have been inferred from the numerical results.

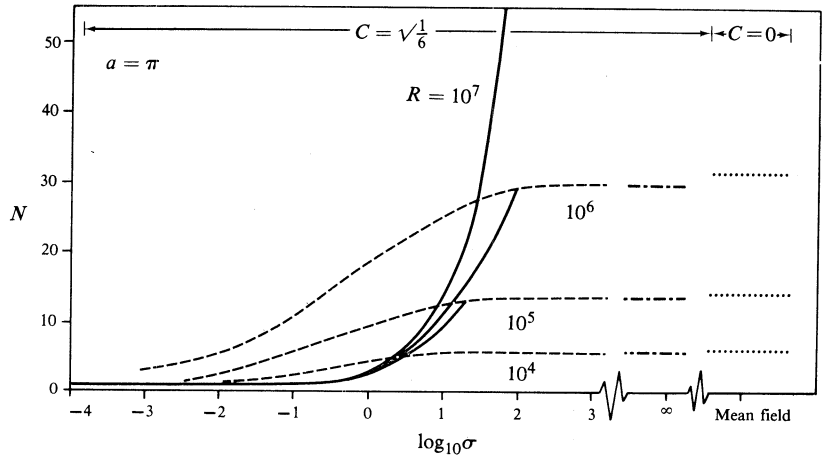

Fig. 1. Variation of the Nusselt number N with $\log_{10}\sigma$ for $a = \pi$ and various values of the Rayleigh number R indicated. The dotted lines correspond to the mean-field equations, the dot–dash lines to $\sigma = \infty$, the dashed curves to type I and solid curves to type II solutions.

When the system is solved with the initial estimates for L_n, the coefficients of the vertical vorticity, all being equal to zero the system converges to what has been termed a type I solution. These are the type described by Murphy (1971) and Toomre *et al.* (1977), where the Z terms have been omitted from the equations in both cases. The N verses σ dependence for these solutions is given in Fig. 1 for various values of R and values of σ in the range $10^{-3} \leqslant \sigma < \infty$, together with the corresponding mean-field solutions. However, when the initial values for the coefficients of the vertical vorticity are nonzero, and R and σ are appropriately chosen, the system converges to a different type of solution. These results establish conclusively that for the same parameter set, there are two distinct solutions of the nonlinear system, convergence to type I or type II being determined by the initial estimates for the coefficients in equations (16). This second type of solution is of the same form as that found by Baker and Spiegel (1975) which they referred to as 'small N', and as that by Van der Borght (1976) which was termed type II, the notation adopted in the present paper. In both of these cases rotation was present, and it was implicitly suggested that rotation was the cause of this non-uniqueness. The type II solutions we have found are clearly not induced by rotation. It is apparent that these type II solutions come about solely due to the extra freedom given to the system by the inclusion of the vertical vorticity.

The main features associated with these type II solutions are that the vertical velocity, and correspondingly the heat flux, measured by the Nusselt number N, are both dramatically reduced from the type I values (see Fig. 1), while horizontal motions are increased and give rise to a cyclonic type flow. Further, the fine boundary layer structure affiliated with type I solutions, which is considered to be difficult to justify on physical grounds (Toomre *et al.* 1977), is substantially dissolved in the corresponding type II solutions.

In addition we have established that type II solutions exist only for certain ranges of R and σ values, with the type I and II solutions coalescing at specific values of R and σ which have been determined numerically when $a = \pi$. Obviously this occurs

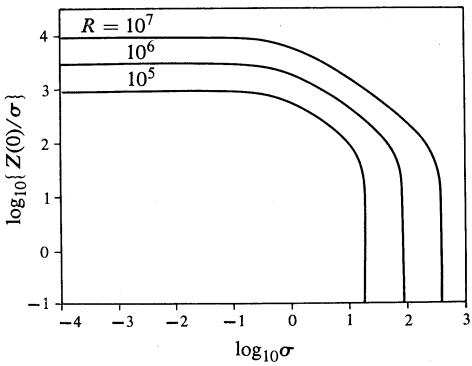

Fig. 2. Variation of $\log_{10}\{Z(z=0)/\sigma\}$ with $\log_{10}\sigma$ for $a = \pi$ and the values of R indicated for type II solutions.

when the Z values from type II solutions go to zero which, as can be seen from Fig. 2, occurs as a sharp cutoff in the $\log_{10}\sigma$–$\log_{10}\{Z(0)/\sigma\}$ plane. The (R, σ) point at which the two solutions coalesce is, for the range of Rayleigh numbers investigated, approximately given by

$$R \sim 10^3\sigma^{1.5}. \tag{25}$$

Furthermore, it is expected that these σ values for any particular R will also be a function of a.

The changes in the physical structure of the type II convective regime with increasing Prandtl number, at fixed Rayleigh number, up to the coalescence of the type II solution with the type I solution is graphically demonstrated in the sequence in Fig. 3. Each part in Fig. 3 shows the projected velocity field structure together with contours of velocity strength (*top*), vorticity field with contours of vorticity strength (*middle*) and the isotherms (*bottom*), all in the xz plane taken at $y = 0{\cdot}25$ with $-2{\cdot}5 \leqslant x \leqslant 2{\cdot}5$ and $R = 10^5$ and $a = \pi$ for a particular σ value. Approximately two hexagonal cell widths are covered by each diagram, a complete cell section and a fraction of the two adjacent cells in the same plane. From Figs 3*a*–3*c*, it is seen that the fluid flow at small σ is essentially swirling horizontally, the projection of the velocity vectors being horizontal, while those corresponding to the vorticity are vertical, which indicates that the velocity must be twisting in the horizontal plane. Also, the associated isotherms are very smooth and reflect the monotonic nature of the mean temperature profile across the layer. As σ is increased the velocity field, which is still essentially horizontal, begins to develop small circulation cells near the top of the layer (Fig. 3*d*) and concurrently the vorticity begins to take on a more horizontal form, especially near the top of the layer. The isotherms now show the development of characteristic thermal plumes, with hot fluid rising in the centre of the cell and cold fluid descending down the sides of the cell. With a further increase in σ, the velocity shows only a small degree of horizontal twisting, the vorticity is almost purely horizontal and the isotherms indicate that significant thermal boundary layers have developed, those at the top of the layer being narrower than those at the bottom. In fact, on comparing Figs 3*g* and 3*h*, for $\sigma = 18$, very little difference between the type I and type II solutions is evident and, when σ is increased further, only one distinct solution exists. The vorticity field is now

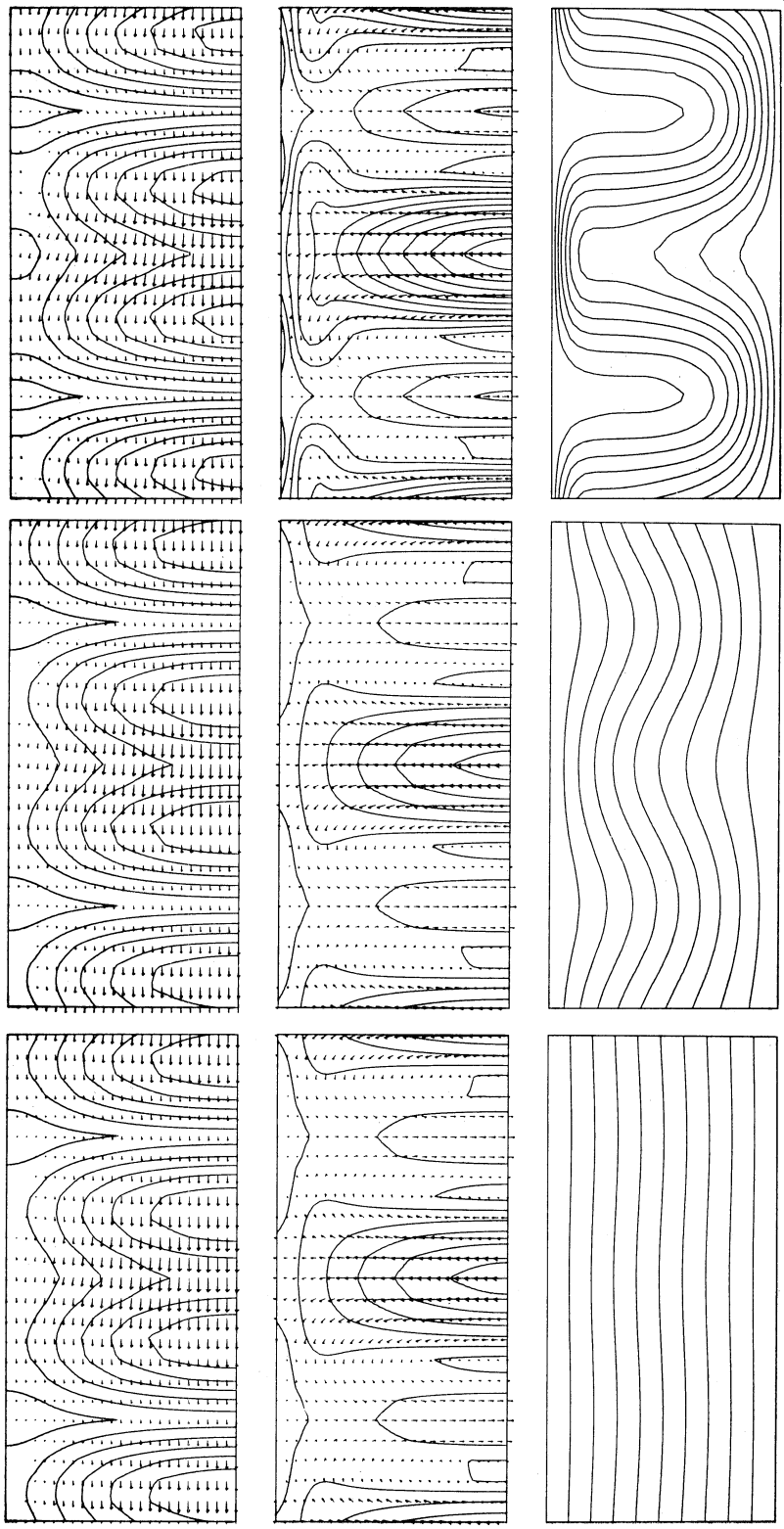

Fig. 3. Projection onto the zx plane at $y = 0{\cdot}25$ for $-2{\cdot}5 \leqslant x \leqslant 2{\cdot}5$ and $0 \leqslant z \leqslant 1$ of the velocity vectors together with contours of $|\boldsymbol{u}|$ (*top*), vorticity vectors together with contours of $|\boldsymbol{\omega}|$ (*middle*) and the isotherms (*bottom*), for $R = 10^5$ and $a = \pi$ for: (*a*) $\sigma = 0{\cdot}01$; (*b*) $\sigma = 0{\cdot}1$; (*c*) $\sigma = 1{\cdot}0$; (*d*) $\sigma = 5{\cdot}0$; (*e*) $\sigma = 15{\cdot}0$; (*f*) $\sigma = 17{\cdot}0$; (*g*) $\sigma = 18{\cdot}0$ (all illustrating type II solutions); and (*h*) $\sigma = 18{\cdot}0$; (*i*) $\sigma = 1{\cdot}0$ (both illustrating type I solutions).

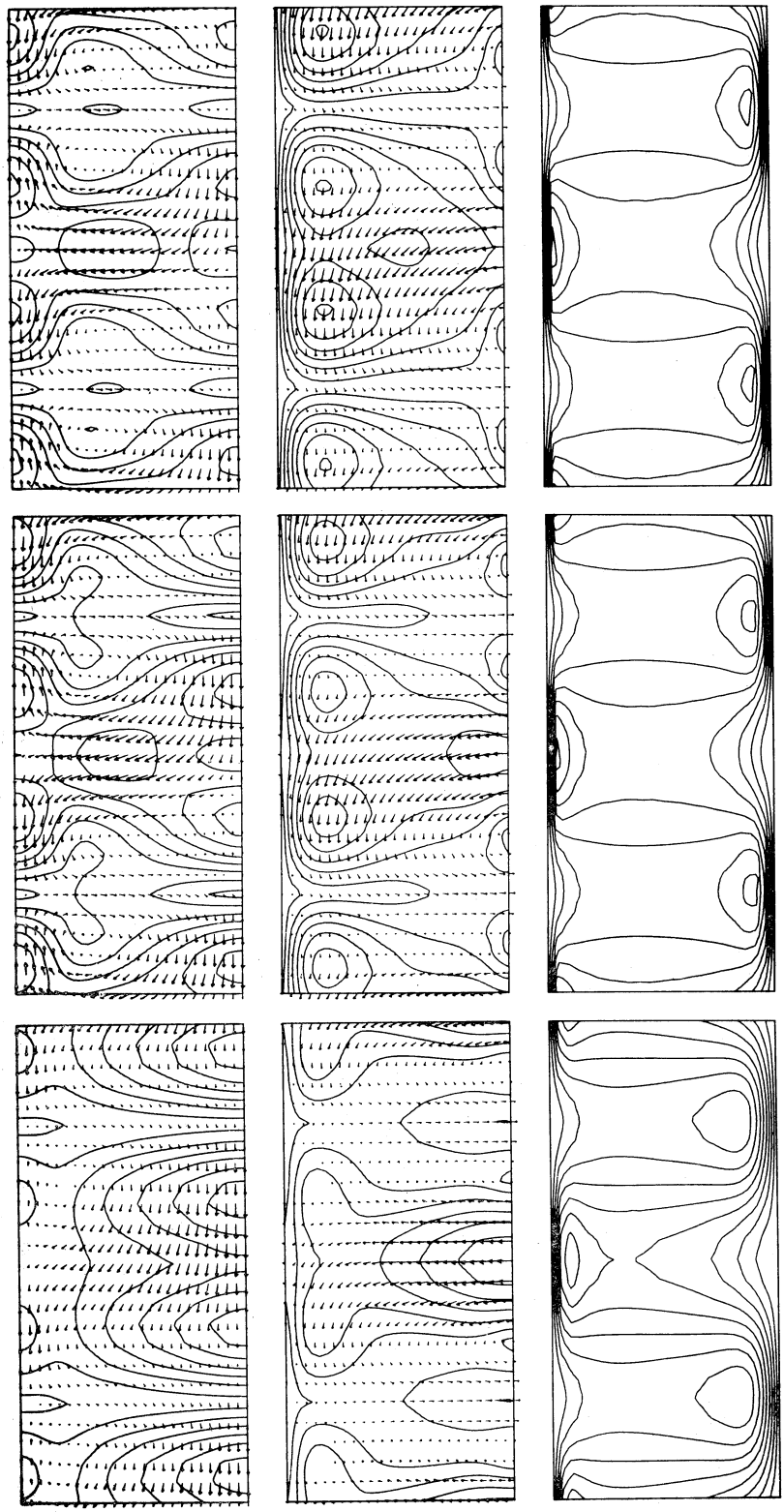

Figs 3*d*–3*f*.

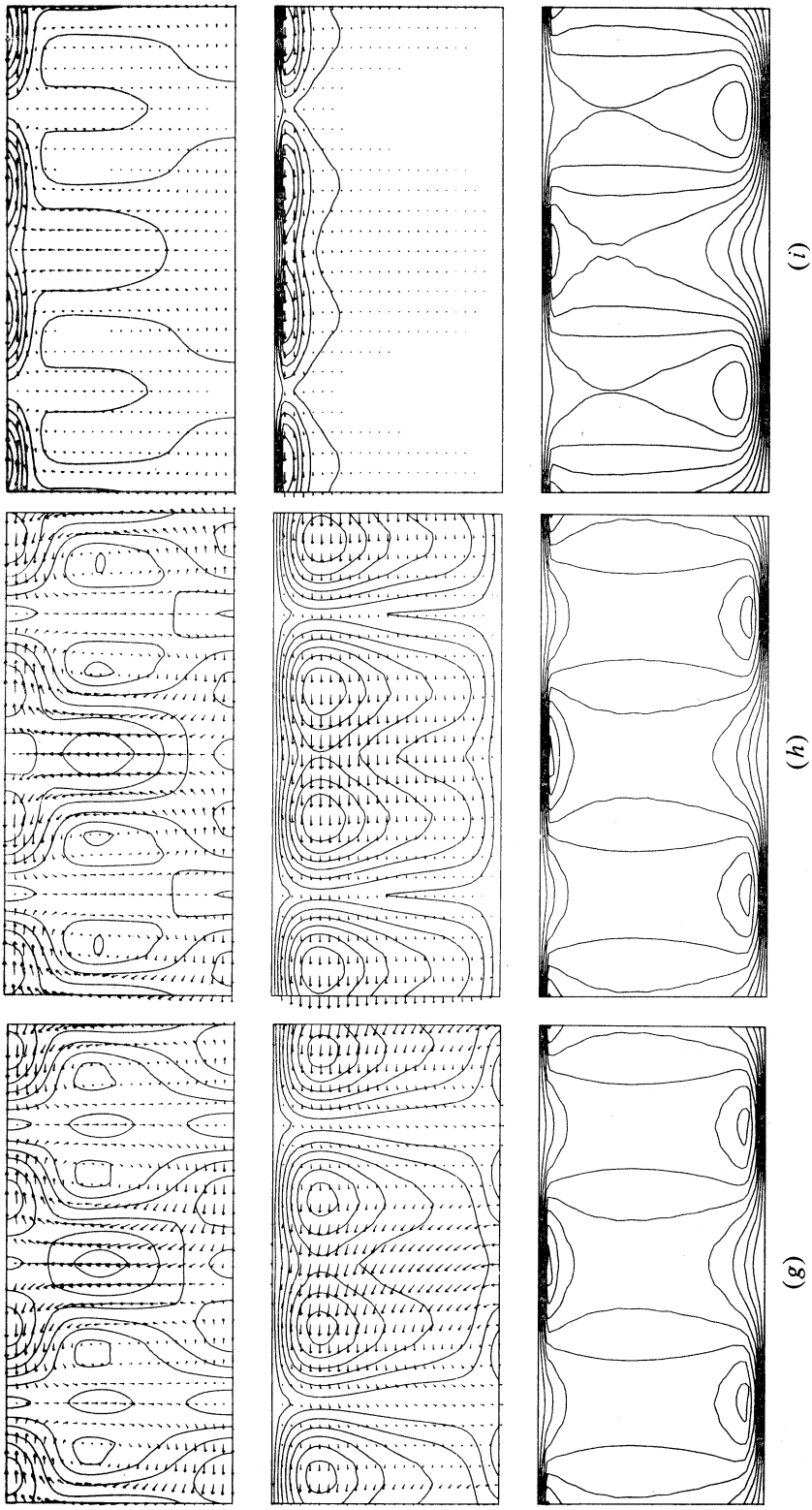

Figs 3g–3i.

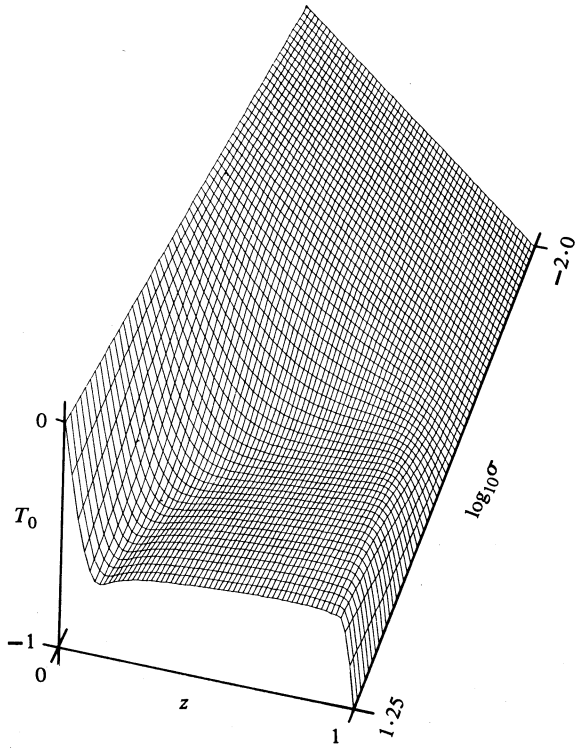

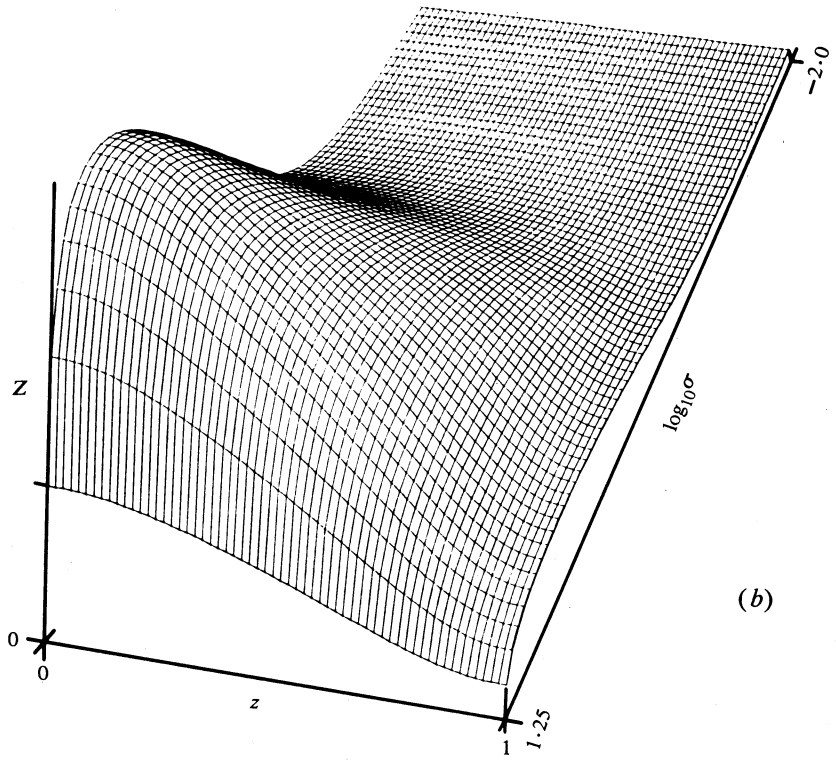

Figs 4*a* and 4*b*. [*see caption p.* 192]

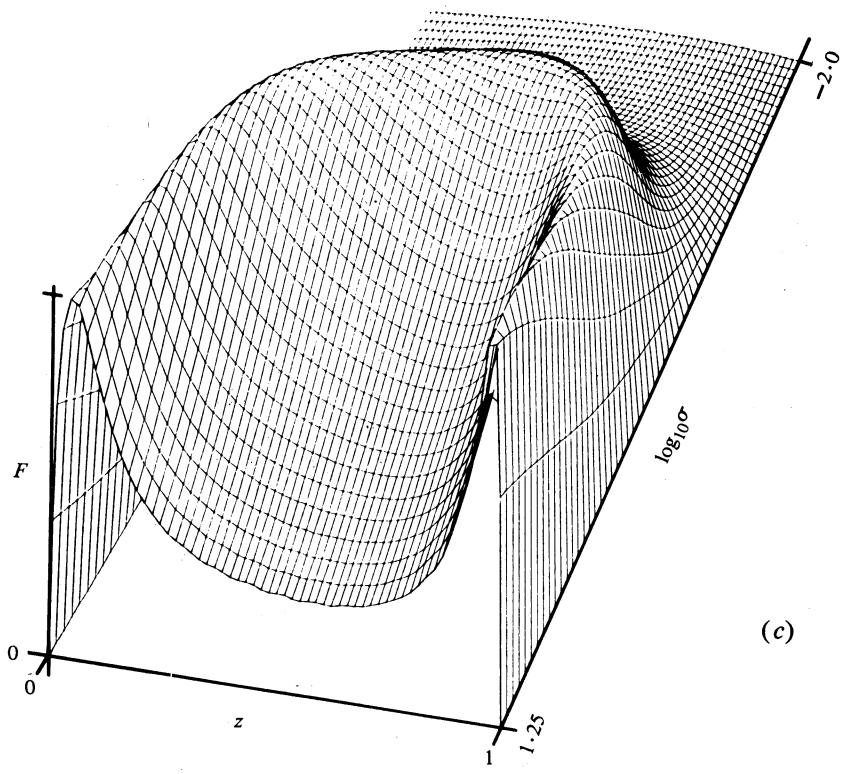

(c)

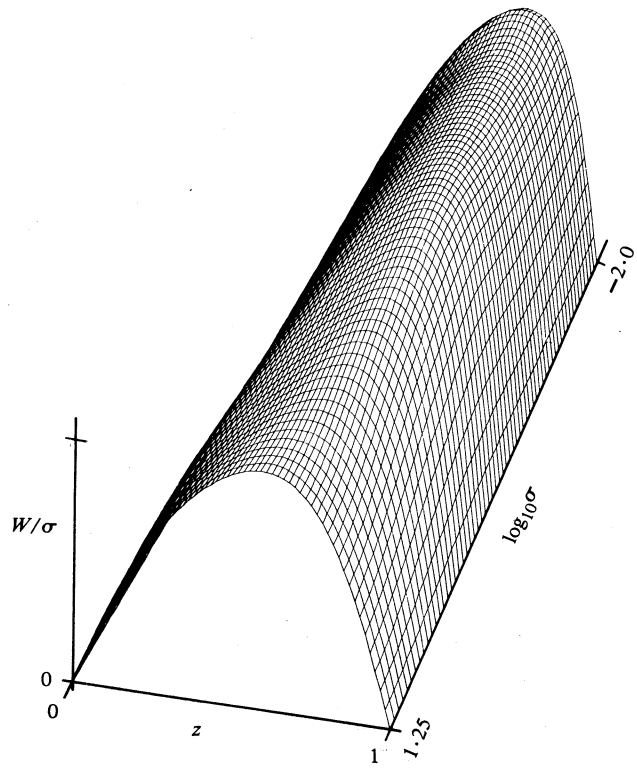

(d)

Figs 4*c* and 4*d*.

completely horizontal and at this point the distinctive type II solution has coalesced into a type I solution, with $Z = 0$. Yet, the difference between the two types is quite dramatic at low σ. Comparing Fig. 3*c*, which is type II, with Fig. 3*i*, which is type I, both obtained for the same set of parameters with $\sigma = 1{\cdot}0$, one finds a completely different flow structure. Whereas in type II the flow is swirling around in a cyclonic manner, the type I flow has the fluid rising up the centre of the cell,

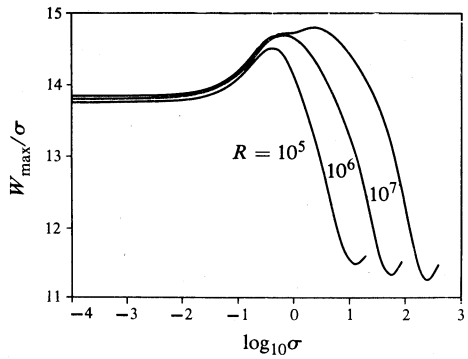

Fig. 5. Variation of the maximum vertical velocity W_{max}, scaled by σ, with $\log_{10}\sigma$ for $a = \pi$ and the values of R indicated for type II solutions.

being diverted by the top of the layer into a fast horizontal radial flow, which is restricted to a thin layer near the top, and then proceeds to flow down the sides of the hexagonal cell. Further, there are regions midway between the centre of the cell and the cell sides where there is virtually no motion. The other striking difference

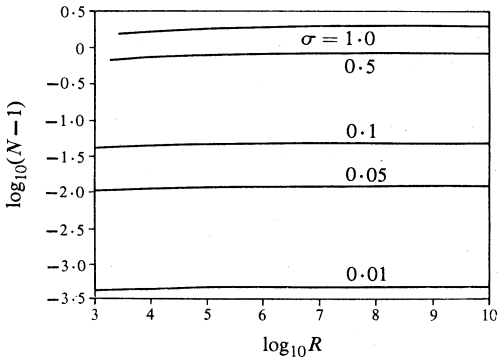

Fig. 6. Variation of $\log_{10}(N-1)$ with $\log_{10}R$ for $a = \pi$ and the values of σ indicated for type II solutions.

is the form of the isotherms, which in type II is mildly distorted from the linear form, whereas in type I it designates the existence of thin thermal boundary layers with an extensive isothermal region in between.

The way in which type II evolves into type I as σ is increased is also graphically demonstrated in Fig. 4, where the functions (*a*) $T_0(z)$, (*b*) $Z(z)$, (*c*) $F(z)$ and (*d*) $W(z)$ are plotted against $\log_{10}\sigma$. At low σ the $T_0(z)$ profile is linear, and as σ increases

Fig. 4. Variation with $\log_{10}\sigma$ at $R = 10^5$ and $a = \pi$ for type II solutions for:
(*a*) the mean temperature profile $T_0(z)$;
(*b*) the vertical vorticity profile $Z(z)$;
(*c*) the temperature fluctuation $F(z)$;
(*d*) the vertical velocity $W(z)$, scaled by σ.

the smooth monotonic dependence on z, which is typical of type II, is evident. Then, for larger values of σ, an extensive isothermal region is established and a 'bump' in the profile is manifest, characteristic of type I $T_0(z)$ profiles. The temperature fluctuation $F(z)$ profile in Fig. 4*c* at low σ is smooth with a single maximum in the layer, and as σ is increased the profile begins to develop two maxima which ultimately develop into the 'rabbit-ear' profile typical of type I and signifies the presence of

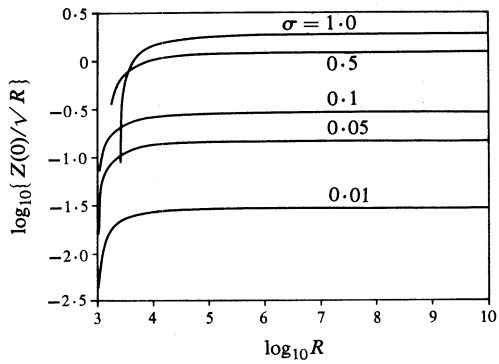

Fig. 7. Variation of $\log_{10}\{Z(z=0)/\sqrt{R}\}$ with $\log_{10}R$ for $a = \pi$ and the values of σ indicated for type II solutions.

thin thermal boundary layers. For the vertical vorticity in Fig. 4*b*, $Z(z)$ is always characteristically nonzero for type II, but as σ becomes large it very quickly tends to zero, indicating a transition towards type I. The velocity profile in Fig. 4*d*, which has been scaled by σ, shows a near constant maximum value, hence $W_{\max} \propto \sigma$ typifies type II solutions. Apart from the amplitude, there is very little dependence of $W(z)$ on σ compared with type I solutions where the maximum in the $W(z)$ profile is shifted considerably towards the upper boundary as σ is reduced.

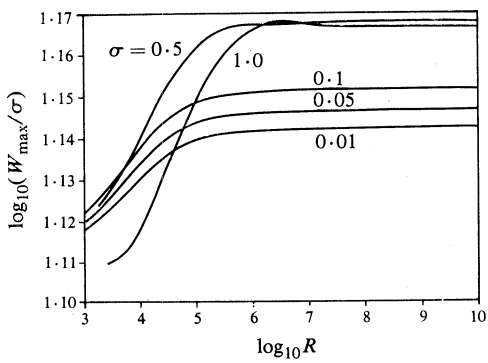

Fig. 8. Variation of $\log_{10}(W_{\max}/\sigma)$ with $\log_{10}R$ for $a = \pi$ and the values of σ indicated for type II solutions.

With astrophysical applications in mind, a prime objective of our numerical computations has been to establish the dependence of N, $W_{\max}$ and $Z(0)$ for type II solutions on R and σ, in this case at constant a. The results obtained are illustrated in Figs 1, 2 and 5–8 and, specifically, the form of these solutions at high R and low σ conveys a near constant trend which in turn allows some general conclusions to be drawn. Figs 5 and 8 confirm again that $W_{\max} \propto \sigma$. Figs 1 and 6 establish that N rapidly tends to the non-convective limit 1 as σ is reduced, for all values of R, which demonstrates that type II solutions are not a very efficient form of convective

heat transport at low values of the Prandtl number. In contrast, the convection of momentum is still a significant feature of type II solutions. From Figs 2 and 7 a reasonable deduction, when $\sigma < 1$ and $R > 10^5$, for the dependence of $Z(0)$ is given by

$$Z(0) \propto \sigma R^{\frac{1}{2}}, \tag{26}$$

with the constant of proportionality probably exhibiting some dependence on the horizontal wavenumber a. The terminal points of the curves on the left side of Fig. 7 designate that as $R \to R_c$ the type II solutions very abruptly lose their separate identity, which is brought about by the vertical vorticity vanishing near these points. To some extent this validates Stuart's (1964) claim that the flow structure of the nonlinear system near the marginal state, $(R-R_c)/R_c \ll 1$, is of the form

$$\boldsymbol{u} = \left((1/k^2)\mathrm{D}W\partial f/\partial x, (1/k^2)\mathrm{D}W\partial f/\partial y, Wf\right), \tag{27}$$

which is independent of vertical vorticity. It may be inferred that the vertical vorticity is very much a nonlinear effect. Further, a perturbation analysis of the form used by Malkus and Veronis (1958) or Veronis (1959), where the variables were expanded in terms of the amplitude of the convection which is assumed to be small, and consequently representing solutions near the marginal state, could not be expected to yield type II solutions.

4. Conclusions

We have established conclusively that the steady-state form of the single-mode equations in certain parameter ranges is capable of giving two distinct solutions, which are not related by any symmetries, when the vertical vorticity terms are included. The existence of these two types of solutions suggests that there must be some selection mechanism to determine which one will ultimately prevail in steady convection. The results of Lopez and Murphy (1982), where the time-dependent magneto-convective system was investigated, strongly suggest that the type I solutions are unstable and the system will evolve to type II solutions which are stable. The different form of boundary layer structure exhibited by the two types of solution also provides supporting evidence for the conclusion.

The consequences of these results may be far reaching when related to astrophysical convection. For example, some areas of penetrative convection may require further examination since the significantly lower vertical convective velocity attributed to the type II solutions would no doubt reduce the extent of overshooting compared with that arising from type I solutions.

In general, results for astrophysical convection which have been based on the modal approximation and do not include the vertical vorticity terms may require revision, since the type II solutions as demonstrated here present a viable alternative, from both the numerical and physical point of view, to the type I solutions over the astrophysical parameter range where R is large and $\sigma \ll 1$. Moreover, we have established that helicity, which is considered to be an essential element of convective dynamos (Moffatt 1977), is inherent in the type II flow structure and does not depend upon rotation as an external constraint.

Further work to be undertaken will establish the dependence of the type II solutions on the horizontal scale, as governed by the horizontal wavenumber a, and to what extent these solutions are a consequence of the stress-free boundaries. The relationship between the form of type II solutions and the nonzero value adopted for C, which depends upon the choice of planform with $0 \leqslant C \leqslant \sqrt{\frac{1}{6}}$, could give a somewhat clearer indication of the role of nonlinear terms for the vertical velocity incorporated in the governing equations.

References

Baker, L., and Spiegel, E. A. (1975). *J. Atmos. Sci.* **32**, 1909.
Busse, F. H. (1972). *J. Fluid Mech.* **52**, 97.
Chandrasekhar, S. (1961). 'Hydrodynamic and Hydromagnetic Stability' (Oxford Univ. Press).
Christopherson, D. G. (1940). *Quart. J. Math. (Oxford)* **11**, 63.
Gough, D. O., Spiegel, E. A., and Toomre, J. (1975). *J. Fluid Mech.* **68**, 695.
Latour, J., Spiegel, E. A., Toomre, J., and Zahn, J.-P. (1976). *Astrophys. J.* **207**, 233.
Latour, J., Toomre, J., and Zahn, J.-P. (1981). *Astrophys. J.* **248**, 1081.
Lopez, J. M., and Murphy, J. O. (1982). *Proc. Astron. Soc. Aust.* **4**, 373.
Malkus, W. V. R., and Veronis, G. (1958). *J. Fluid Mech.* **4**, 225.
Moffatt, H. K. (1977). 'Magnetic Field Generation in Electrically Conducting Fluids' (Cambridge Univ. Press).
Murphy, J. O. (1971). *Proc. Astron. Soc. Aust.* **2**, 53.
Stuart, J. T. (1964). *J. Fluid Mech.* **18**, 481.
Toomre, J., Gough, D. O., and Spiegel, E. A. (1977). *J. Fluid Mech.* **79**, 1.
Toomre, J., Zahn, J.-P., Latour, J., and Spiegel, E. A. (1976). *Astrophys. J.* **207**, 545.
Van der Borght, R. (1976). *Aust. J. Phys.* **29**, 305.
Van der Borght, R., and Murphy, J. O. (1973). *Aust. J. Phys.* **26**, 617.
Veronis, G. (1959). *J. Fluid Mech.* **5**, 401.
Zahn, J.-P., Toomre, J., and Latour, J. (1982). *Geophys. Astrophys. Fluid Dyn.* **22**, 159.

Manuscript received 8 August, accepted 11 November 1983